Computational Experiments on Filled Rubber Viscoelasticity: What Is the Role of Particle−Particle Interactions?

Guido Raos,* Margherita Moreno, and Stefano Elli

Dipartimento di Chimica, Materiali e Ingegneria Chimica "G. Natta", Politecnico di Milano, Via L. Mancinelli 7, I-20131 Milano, Italy

Received May 5, 2006; Revised Manuscript Received July 18, 2006

ABSTRACT: We present the results of computer simulations of model polymer networks containing stiff and roughly spherical colloidal particles at 20% volume fraction. We employ the coarse-grained "dissipative particle dynamics" model (DPD). The filler particles may be either well dispersed or aggregated, and the strength of their interaction can be tuned by changing the parameters of the polymer−filler nonbonded potentials. By performing nonequilibrium molecular dynamics simulations, we are able to probe directly the viscoelastic behavior of the composites under oscillatory shear deformations of variable amplitude and frequency. The strength of the particle−particle interactions and sample morphology has a certain effect on the small-strain moduli. In some cases, we also observe a nonlinear viscoelastic behavior as a function of increasing shear amplitude. However, the characteristics of this nonlinearity are different from the experimentally observed "Payne effect". Therefore, the origin of this effect does not seem to be entirely and directly related to particle−particle interactions, as is frequently assumed.

1. Introduction

Despite its practical importance and the large bulk of empirical knowledge accumulated over the years, the microscopic origin of rubber reinforcement by rigid colloidal fillers such as carbon black and silica is still a largely unsettled question.[1−4] For a given volume fraction ϕ of reinforcing filler (talc is considered nonreinforcing, to give one counterexample), only a fraction of the increase in the modulus can be understood by assuming some kind of "additivity" of the properties of the rubber and filler phases, as in the Einstein−Smallwood−Guth formula for the so-called hydrodynamic effect:[5]

$$G = G_0(1 + 2.5\phi + ...) \quad (1)$$

where G and G_0 are the shear moduli of the composite and the rubber matrix, respectively. Equation 1 can be derived for rigid spherical particles at small concentrations, under the assumption that there is perfect adhesion at the interface and the properties of each phase are everywhere identical to those in the bulk. It can be generalized in a number of ways to describe composites at high concentrations.[6−9] Scaling arguments can also be used to extend it from spherical to highly branched fractal fillers.[10−12] Despite their relative sophistication, even these theories cannot account fully for the measured elastic moduli, which can easily be 10−50 times larger than that of the matrix. Therefore, something seems to be missing from the basic physical model.

An early but still popular interpretation of the "extraordinary" reinforcement by carbon black and silica ascribes a large fraction of small-strain elastic modulus of filled rubbers to interparticle forces.[1−4] This picture is not unreasonable, since such forces are well-known to exist and to have significant implications for the whole of colloid science.[13] Also, since these particle−particle interactions will be somehow disrupted on going to increasingly large deformations, they have been invoked to explain the observed softening of the material at small−moderate strains (Payne effect[2]). The breakup of the filler aggregates under strain has been recently observed by in-situ microscopy experiments, which have also provided an estimate of their mechanical strength.[14] Thus, this particle−particle interaction picture has the appealing feature of "killing two birds with one stone", by invoking the same basic mechanism to explain both the large modulus at small strains and its drop at increasing deformations. These considerations can also be used as a basis for semiquantitative interpretations of the frequency and deformation dependence of the complex shear modulus ($G^* = G' + iG''$).[15−17] However, the status of these models remains unsettled due to the unavoidable introduction of adjustable parameters.

In recent years, it has become increasingly apparent that the previous picture is at least incomplete. The development of silica fillers, which need to be made compatible with the polymer by chemical functionalization and covalent linkage,[18] has demonstrated the importance of good dispersion and adhesion at the rubber−filler interface. These could somehow be taken for granted in the case of carbon black. At the same time, there has been increasing evidence of the formation of a glassy polymer layer at the interface with the filler.[4,19−21] Since the thickness of this rigid polymer shell can be of the order of a few nanometers, its volume will be comparable to that of the particles when these are also nanoscopic. The resulting increase in the effective volume fraction of rigid material (filler and glassy polymer) has been shown to go a long way toward justifying the very large values of the small-strain modulus, at least in some cases.[12] Therefore, particle−particle interactions, although certainly present, might not be so important after all. Or, perhaps, their interpretation needs to be revised. For example, some authors have suggested that the main mechanism at the basis of filler networking is not a van der Waals-type interaction,[13,17] but is the bridging of the particles by strongly adsorbed polymer chains.[22,23] Therefore, the interaction is not "direct", but is mediated by the polymer. But, if that is the case, what is the origin of the nonlinearities at large cyclic deformations? Some alternatives to the "particle−particle interaction" interpretation of the Payne effect have been proposed. These

* Corresponding author: ph +39-02-2399-3051; fax +39-02-2399-3080; e-mail guido.raos@polimi.it.

10.1021/ma061008h CCC: $33.50
Published on Web 08/22/2006

include the adsorption−desorption dynamics of the chains,[24] the release of trapped entanglements at the polymer−filler interface,[25] and the plasticization of the glassy rubber shell bridging neighboring filler particles.[20]

Computer simulation by molecular dynamics (MD) and Monte Carlo (MC) methods has been increasingly used to gain a better understanding of polymer-based nanocomposites.[26−33] These simulations have provided, for example, further evidence of the formation of a glassy shell coating the particles. They have also been used to investigate the conformational statistics of the chains at the surface and of the "bridges" connecting different particles, which are not easily accessible by experiment. These molecular-level studies are complemented by continuum-level simulations using, for example, the finite element method (FEM).[34] This allows a fast and reliable estimate of the elastic moduli of a composite from the knowledge of the sample morphology and the elastic properties of the individual phases.[35] However, the continuum approach has also some shortcomings: the FEM can encounter difficulties for large deformations (an important issue when dealing with rubbery materials, as opposed to ceramic- or metal-based composites), it neglects from the outset the possibility of long-range interactions among colloidal particles,[13] and its common assumption of constancy and transferability of the properties of the individual phases[6,7] may be untenable close to the rubber−filler interface. Thus, it is fair to say that we are still far from the development of a comprehensive computational method for the simulation of filled elastomers, but it seems likely that this will need to combine features of the molecular-level and the continuum-level approaches.

The aim of the present work is to use computer simulation to test some general ideas about the behavior of filled rubbers. We employ a model which, despite its relative simplicity, captures some important aspects of real systems which were neglected by previous simulation studies: (i) the filler particles do not have simple idealized geometries (spheres or regular polyhedra) but have a somewhat irregular shape and surface topography; (ii) the particle may have different degrees of dispersion/agglomeration within the polymer and different degrees of affinity for the polymer matrix; (iii) the polymer matrix is not a melt of linear polymer chains, but it is a fully developed cross-linked network; (iv) in close analogy with experimental investigations, we probe directly the behavior of the composite under cyclic shear deformation by nonequilibrium molecular dynamics. All this is made possible by the adoption of the "dissipative particle dynamics" (DPD) model[36]—a coarse-grained simulation method which has already been successfully applied to other problems in polymer physics.

Section 2 contains a description of our computational procedures, while our main results are presented in section 3. Conclusions follow.

2. Computational Methods

Dissipative Particle Dynamics (DPD). Similarly to conventional molecular dynamics (MD), DPD is a particle-based simulation approach. It is coarse-grained, in that each dissipative particle actually represents a group of several atoms (roughly of the order of five CH_2 units). As we shall see, a colloidal filler "particle" will be modeled by several hundred dissipative "particles". We shall use the terms "particle" for the former and "atoms" for the latter, so as to avoid any ambiguity without introducing too cumbersome terminology.

References 36 and 37 contain exhaustive descriptions of the DPD method. The latter also describes some selected applications to soft matter problems, such as the phase behavior of block copolymers or the structure and dynamics of lipid bilayers and micelles, as well as recent technical developments such as new integration algorithms. We have used a fairly standard version of the method, as implemented in the coarse-grained MD program COGNAC.[38] We refer the reader to the original publication[36] for a description of the DPD thermostat and integration algorithm.

In DPD, it is convenient to work with reduced quantities. All atoms have the same interaction range (or diameter, for short) σ, which sets the unit of length. In other words, we take $\sigma = 1$. Similarly, the unit of mass is taken such that all atoms have mass $m = 1$. Finally, the temperature and energy scales are defined such that $k_BT = 1$. All other quantities can be derived from these three fundamental units. For example, the number density of atoms ρ is measured in σ^{-3} units. Following the recommendations of Groot and Warren,[36] we have conducted all simulations at $\rho = 3$. Time is measured in units of $\tau = \sigma(m/k_BT)^{1/2}$. Pressure, stress, and elastic moduli are measured in k_BT/σ^3 units.

In the notation of ref 36, we have used a DPD thermostat with the friction/noise parameter $\gamma = 4.5$. The equations of motion were integrated with the modified velocity-Verlet scheme with $\lambda = 0.65$ and a time step $\Delta t = 0.05\tau$. These correspond to the default parameter settings and recommendations of ref 36. However, since the use of long time steps has been recently shown to be a possible source of artifacts[39] and there is also a concern that the thermostat might affect the system's response under shear, we shall also present the results of a few test simulations with shorter time steps and/or smaller values of the γ parameter.

Interaction Potentials. The bonded and nonbonded interactions between the filler (F) and polymer (P) atoms are described by very simple functional forms. In particular, the bond potentials are harmonic:

$$V_{FF}^{BOND}(r) = \frac{1}{2}k_{FF}(r - r_0)^2,$$

$$V_{PP}^{BOND}(r) = V_{PF}^{BOND}(r) = \frac{1}{2}k_{PP}r^2 \qquad (2)$$

Thus, the polymer−polymer and polymer−filler bond are taken to be identical, with a standard[36] force constant $k_{PP} = 4$. The filler−filler bonds are characterized by a stiffer force constant ($k_{FF} = 60$), and they have a nonzero equilibrium bond length $r_0 = 0.7071$. We have adopted a nonzero bond length in order to ensure that the filler particles, which are heavily cross-linked by several FF bonds per bead (see below), retain a finite size instead of shrinking to almost pointlike globules upon cross-linking (as predicted by the theory of 3D phantom networks[40]). The specific value $r_0 = 0.7071$ was chosen to be roughly consistent with the distribution of nearest-neighbor distances in a melt of DPD beads at the density $\rho = 3$.

The nonbonded interactions are described by soft repulsive potentials:[36]

$$V_{IJ}^{NB}(r) = \begin{cases} \frac{1}{2}a_{IJ}(r - \sigma)^2, & r \le \sigma = 1 \\ 0, & r \ge \sigma = 1 \end{cases}$$

This potential is entirely specified by the a_{IJ} parameter. Values of a_{IJ} in the range 25−100 (in k_BT/σ^2) are usually employed. Unlike conventional MD with "hard" repulsive short-range potentials, the softness of the DPD interactions implies that two

Table 1. Definition of the a_{IJ} Nonbonded Interaction Parameters Used in Each Simulation[a]

	P−P	F′−F′	F″−F″	P−F′	P−F″	F′−F″
case I	50	50	50	72	72	50
case II	50	50	50	50	72	72
case III	50	50	50	50	50	50

[a] F′ and F″ represent two types of filler atoms (which are identical in cases I and III), while there is only one type of polymer atom (P).

particles may be easily found at a distance significantly smaller than their diameter. Compenetrability of the particles means that entanglement constraints are not rigorously respected in a liquid or a network of DPD chains. For similar reasons, these model systems are not expected to undergo a sharp glass transition at low temperatures (roughly speaking, a liquid becomes "glassy" when the atomic motions become severely restricted by the surrounding amorphous material). These features of DPD are not necessarily a disadvantage, if they are exploited judiciously. For example, they allow relatively long time steps in dynamical simulations and fast equilibration of complex multiphase systems.

Although the two-body potential between any pair of atoms is always repulsive ($a_{IJ} > 0$), an *effective* many-body attraction can still be modeled by playing with the relative values of these parameters, so that some interactions are "less repulsive" than others.[36,37] In fact, the DPD nonbonded potentials have even been shown to be flexible enough to model specific systems, such as polymer blends (there is an approximate relationship between the a_{IJ}'s and Flory's χ parameter[36]) or even cell membranes interacting with nonionic surfactants in water.[41] Since our present aim is to gain an understanding of some very general features of filled rubber, we have used typical but generic values, without carrying out any fine-tuning of the parameters. Specifically, we have simulated three different systems (see Table 1). Case I represents a situation with strongly repulsive polymer−filler interactions. Therefore, the filler is incompatible with the polymer, and this results in attractive and relatively strong interparticle forces. In case III, all the a_{IJ} parameters are identical so that the polymer is identical to the filler from the point of view of nonbonded interactions (but there is still a large difference in their mechanical stiffness because of our choice of bonding potentials). This models a situation in which the filler surface has been made maximally compatible with the polymer by chemical functionalization, and particle−particle interactions are virtually absent. Finally, in case II there are two types of filler atoms (F′ and F″), half of which are identical to the polymer atoms, whereas the other half is incompatible with them. This models an intermediate situation with attractive but weaker interparticle forces. Moreover, in case II the particle surfaces are chemically heterogeneous—a situation which occurs frequently with fillers such as carbon black and precipitated silica.

System Preparation. The preparation of the cross-linked nanocomposites is a important step in the simulation and was performed by the steps illustrated in Figure 1. Note that we always used the case I potentials during this stage. We switched to case II or case III potentials only afterward, in the nonequilibrium simulations of viscoelastic response (see below).

We started from a random mixture of 1300 linear chains of polymer-like atoms (P_{14}) and 600 triblock chains containing a central block of filler-like atoms ($P_{14}F_8P_{14}$).[42] This composition corresponds to a filler volume fraction $\phi = 0.12$. The unfavorable polymer−filler interactions cause formation of nearly spherical F-rich micelles. We transformed these micelles into solid filler particles by creating a large number of F−F bonds between neighboring filler atoms (up to a maximum valency of 12 bonds per atom). We then deleted most of the P_{14} chains (only 170 were left) and gradually reduced the size of the simulation box so as to increase the filler volume fraction to $\phi = 0.20$ and bring the density back to the desired value $\rho = 3$ (final cubic box side $L = 19.99$).[43] Finally, we cross-linked the polymer matrix by forming bonds between the free polymer terminals and randomly selected inner monomers of the polymer strands.[44] This readily produces a fully developed network with trifunctional junctions. Note that have deliberately chosen to produce a tightly cross-linked network with short primary chains to compensate for the absence of entanglement effects in DPD. The final system contains 19180 P-type atoms and 4800 F-type atoms. There are 18 distinct and well-dispersed filler particles of variable size, roughly comprised between 100 and 500 atoms.

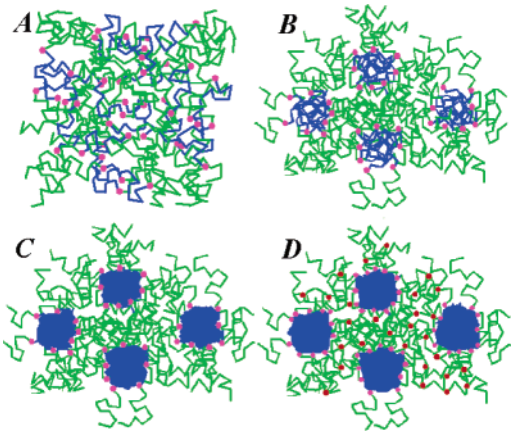

Figure 1. Pictorial description of the procedure for the generation of the system with dispersed filler particles. The starting configuration (frame A) contains a random mixture of $P_{14}F_8P_{14}$ triblock and P_{14} homopolymer chains. The P strands are depicted in green, the F strands in blue, and the P−F bonds by the magenta dots. The F-blocks aggregate into micelles (frame B), which are then transformed into solid particles by formation of many additional F−F bonds (frame C). Finally, the particle volume fraction is increased up to $\phi = 0.20$ (not shown), and the loose ends of the polymer are also allowed to react to form a cross-linked polymer matrix (the cross-links are the red dots in frame D).

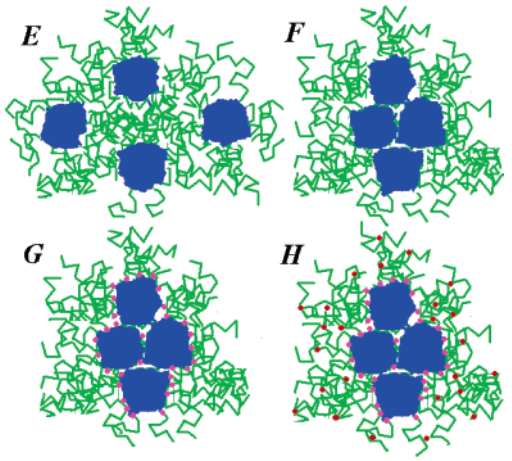

Figure 2. Pictorial description of the procedure for the generation of the system with aggregated filler particles. Starting from configuration C of Figure 1 ($\phi = 0.20$), we cut all P−F bonds (frame E) and as a result the filler particles aggregate (frame F). Finally, we regenerate the P−F bonds (magenta dots in frame G) and cross-link the polymer matrix (red dots in frame H).

To generate an analogous system with aggregated filler particles, we followed the procedure depicted in Figure 2. Starting from the previous system at the stage before the final cross-linking, we simply cut all P−F bonds. Without the tethered

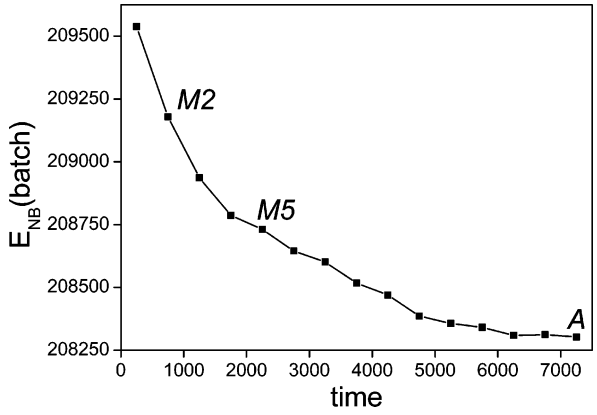

Figure 3. Evolution of the nonbonded potential energy of the nanocomposite (batch average) during the aggregation of the filler particles. The points used for the subsequent simulations have been marked by M2, M5, and A.

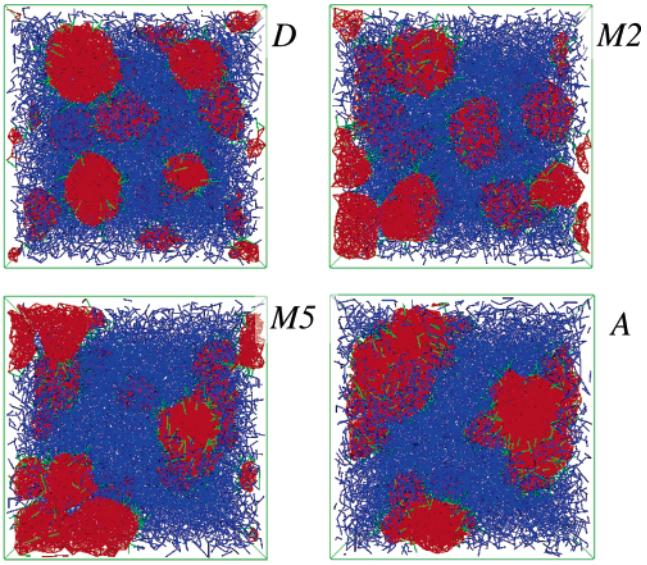

Figure 4. Snapshots of the systems with dispersed (D), moderately aggregated (M2 and M5), and fully aggregated (A) filler particles. The F−F bonds are drawn in red, the P−P bonds in blue, and the P−F bonds in green. The M2, M5, and A systems correspond to the second, the fifth, and the last points in Figure 3, respectively.

polymer shell surrounding them, the particles diffuse and aggregate. Aggregation can be easily monitored from the decrease of the nonbonded energy of the system during the simulation, shown in Figure 3. By re-forming the P−F bonds at different stages of this process and cross-linking the polymer matrix, we were able to produce an ensemble of systems with different degrees of particle−particle aggregation.

Figure 4 shows a snapshot of the four morphologies which were selected for subsequent nonequilibrium simulations under shear. These will be indicated by D (for dispersed), M2 and M5 (for moderately aggregated), and A (for fully aggregated). We point out that, since these pictures represent the unit cell of an infinite system with periodic boundary conditions, the filler particles in system A actually form a single very large aggregate.

For comparison purposes, we also carried out simulations of an unfilled network made up of P_{14} chains, which were cross-linked by the same procedure used for the filled samples.

Nonequilibrium Simulations. We studied the viscoelastic properties of the cross-linked nanocomposite samples by applying an oscillatory shear deformation and recording the resulting stress. The oscillatory shear deformation was applied through the "sliding brick" or Lees−Edwards boundary conditions[45] and is characterized by the amplitude γ_0 and the frequency ν:

$$\gamma_{xy}(t) = \gamma_0 \sin(2\pi\nu t) \tag{3}$$

We used the values $\gamma_0 = 0.025$, 0.05, 0.10, 0.20, 0.40, and 0.80 (i.e., from 2.5% to 80%) and $\nu = 10^{-3}$ and 10^{-4} (in τ^{-1} units). These two frequencies were selected by trial and error so as to have tan $\delta \cong 0.05-0.4$ (see below), which is the typical range for a filled elastomer operating at room temperature and frequencies of $10^{-1}-10^{2}$ Hz.[1−4] The simulations generally lasted up to completion of 5−10 deformation cycles. Just as in the static simulations, the system's temperature was automatically kept around the desired value $k_BT = 1$ by the DPD equations of motion. (Heat has to be removed from the system, since the imposed shear deformation corresponds to an input of mechanical work.) The DPD method has a built-in thermostat, which has been shown to be quite efficient for nonequilibrium simulations.[45,47]

The resulting stress (both instantaneous values and batch averages over a certain number of time steps) was calculated by the program and stored in a file. The output frequency was adjusted to the deformation frequency, so as to record 50 values of the stress every cycle. These were subsequently analyzed by fitting them as follows:

$$\sigma_{xy}(t) = \sigma' \sin(2\pi\nu t) + \sigma'' \cos(2\pi\nu t) \tag{4}$$

The σ' and σ'' parameters can then be converted into the in-phase and out-of-phase components of the complex modulus (G' and G'') and their ratio (tan δ):

$$G' = \frac{\sigma'}{\gamma_0} \qquad G'' = \frac{\sigma''}{\gamma_0} \qquad \tan\delta = \frac{G''}{G'} = \frac{\sigma''}{\sigma'} \tag{5}$$

3. Results and Discussion

Since we are interested in probing the effect of the particle−particle interactions and these depend both on their degree of aggregation (D, M2, M5, or A—see Figure 4) and on the interatomic nonbonded potentials (I, II, or III—see Table 1), we shall use a combined symbol to denote the different simulations. For example, D−I corresponds to the system with dispersed particles and case I potentials, while A−III indicates the system with aggregated particles and case III potentials.

Representative plots of the time dependence of the shear stress for system D−I are provided in Figure 5. They correspond to the extreme cases of slow, small-amplitude deformations ($\gamma_0 = 0.05$, $\nu = 10^{-4}$) and fast, large-amplitude deformations ($\gamma_0 = 0.80$, $\nu = 10^{-3}$). We have plotted both the instantaneous values of the stress at regularly spaced instants of time (once every 4000 or 400 DPD integration steps respectively for the low- and high-frequency simulations) and their batch averages over all the time steps within each of these intervals.[48] In the case of large deformations, the instantaneous values make relatively minor deviations from the batch averages. Both appear to follow closely the sinusoidal law in eq 4. In the case of small deformations, instead, the instantaneous values of the stress take apparently random values. As a matter of fact, negative shear stresses are frequently recorded at positive deformations, and vice versa. These wild fluctuations are clearly due to thermal noise, mainly introduced through the DPD thermostat. Fortunately, the batch averages do not suffer from this problem and they appear to follow closely eq 4. Even so, we are unable to simulate reliably deformations of 0.1−1%, which are instead accessible to experimentalists. This is a limitation of our current

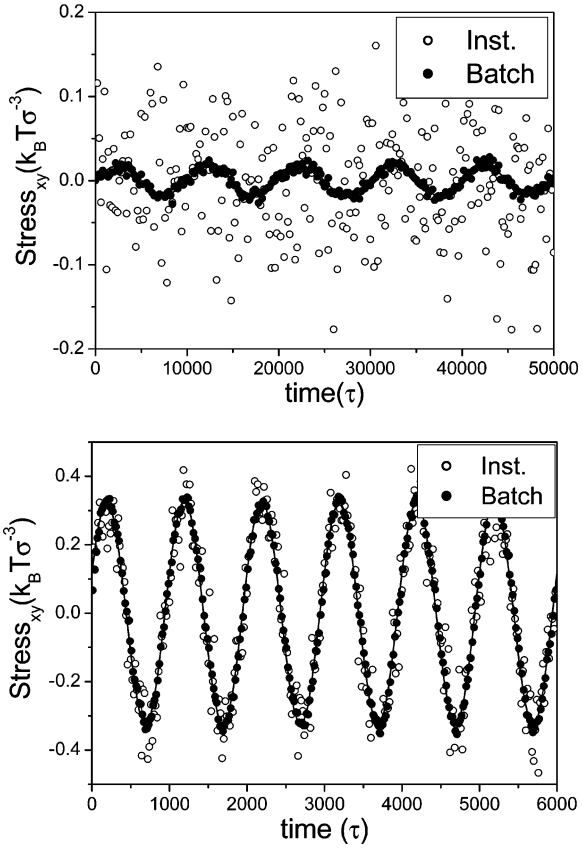

Figure 5. Plots of the shear stress for system D−I, for $\gamma_0 = 0.05$ and $\nu = 10^{-4}\tau^{-1}$ (top) and for $\gamma_0 = 0.80$ and $\nu = 10^{-3}\tau^{-1}$ (below). The continuous lines are sinusoidal fits to the black points (batch averages). The instantaneous values of the stress are indicated by the empty dots.

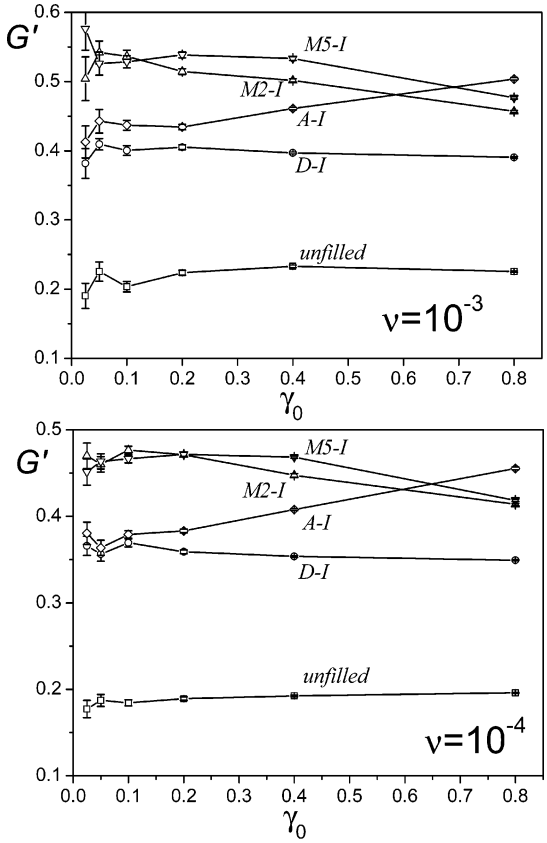

Figure 6. In-phase component of the modulus as a function of shear amplitude, for systems with different morphologies (D, M2, M5, and A) but identical interaction potentials (case I).

simulations, which could be overcome by studying much larger systems over much longer times in order to reduce the noise/signal ratio.

The stress vs time plots such as those in Figure 5 show that the response of our model systems in first deformation cycle is very similar to that in the following ones. This does not occur in real filled rubbers, where the elastic modulus in the first deformation cycle is significantly larger than in the following ones (Mullins effect[3]). Presumably, the perfect reversibility and history independence of the our stress−strain curves is due to the lack of any "damage" mechanism in our model (chain scission or rubber-filler debonding, for example).

The G' and G'' components obtained from eqs 4 and 5 have identical error bars, in absolute terms. However, since G' is 3−20 times G'' depending on deformation frequency, their relative values are much larger in the latter case.[49] For this reason we shall restrict our discussion to the in-phase or elastic components of the moduli (henceforth, "the modulus"), which have been plotted in Figures 6 and 7. First of all, we observe that the modulus of the unfilled sample (G_0') is almost perfectly independent of the deformation amplitude, in agreement with experiment. A 10-fold increase in frequency produces a 10% increase in the modulus. This effect is observed also in the simulations of the filled samples and is quite reasonable from a physical point of view. Apart from this shift, the behavior at $\nu = 10^{-3}$ always parallels that at $\nu = 10^{-4}$, and consequently there is no need to refer to a specific frequency in the following discussion.

If we compare the small-strain moduli ($\gamma_0 \leq 0.2$) of systems with identical polymer−filler interaction potentials but different morphologies (Figure 6), we observe an interesting nonmonotonic behavior of G'/G_0'. Systems A and D, where the particles are either completely aggregated or very well dispersed, have similar values of this ratio (1.8−1.9). This is close enough to 1.7, predicted by the Christensen−Lo model[6,12] from the sole knowledge of the filler volume fraction. The moduli of the M2 and M5 systems with moderately aggregated particles are significantly larger ($G'/G_0' = 2.3-2.5$). The reason for this difference is that in the latter case the particles form a tenuously connected structure which spans a larger volume within the sample. This increases the effective volume fraction of filler, since the polymeric material contained within this spanned region is somewhat screened from deformation.[4,11,12] On the other hand, when the particles are completed aggregated, they form a very compact object with no or little polymer in between. This large aggregate effectively behaves as a single near-spherical particle, which explains the similarity between the A and D cases.

The Payne effect corresponds to a drop in the elastic modulus by about 1 order of magnitude at very small deformations (roughly up to $\gamma_0 = 0.05$).[1−4] This characteristic nonlinear behavior does not occur in our simulations: allowing for the error bars, which as explained above are more significant at small deformations, the modulus is roughly strain-independent up to $\gamma_0 \cong 0.2$. The *D* sample has a perfectly linear response also for $\gamma_0 > 0.2$, just like the unfilled rubber (see again Figure 6). Nonlinearities at medium and large deformations show up when the particles are moderately or fully aggregated. The overall change in the modulus is small compared to order-of-magnitude drop observed experimentally.[1−4] Still, it is interesting that the modulus of M2 and M5 decreases while that of A increases, so that these curves cross at $\gamma_0 \cong 0.65$. We may conventionally refer to these types of behavior as Payne-like

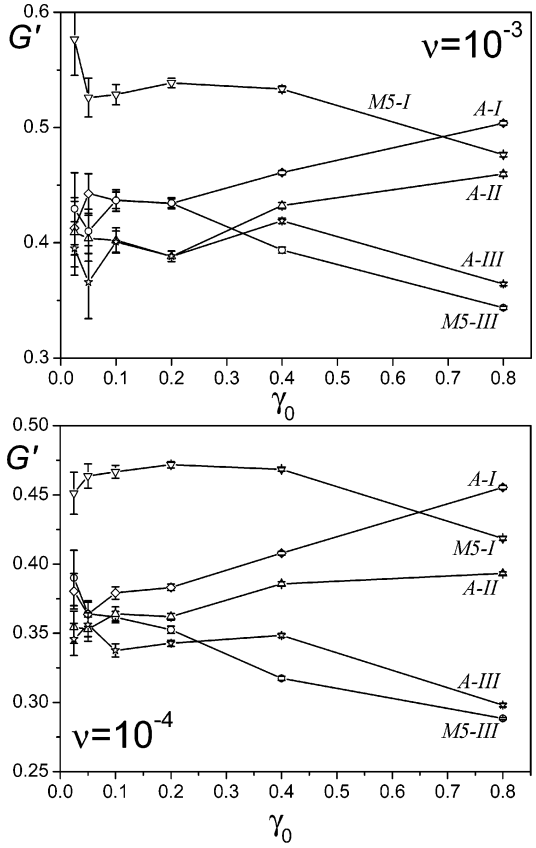

Figure 7. In-phase component of the modulus as a function of shear amplitude, for systems with aggregated morphologies (M5 or A) and different interaction potentials (cases I, II, and III). The curve for the unfilled network (given in Figure 6) has been omitted for clarity.

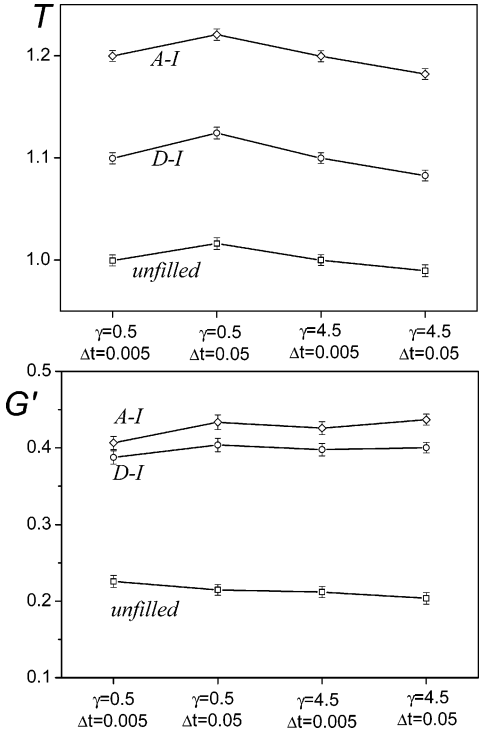

Figure 8. Test of the effect of the DPD friction/noise parameter γ and of the time step Δt on the values of the temperature (above) and of the in-phase shear modulus (below). All the plots have been obtained in shear experiments with frequency $\nu = 10^{-3}$ and amplitude $\gamma_0 = 0.1$. The temperature plots for the two filled systems have been upshifted by 0.1 and 0.2, for clarity. The error bars represent the standard deviation of the temperature fluctuations and the estimated error in the modulus, respectively.

and anti-Payne, respectively. A possible explanation of the former is that, on going to increasingly larger deformations, we are breaking up the loosely connected network of filler particles. The more open aggregates, which shield a significant fraction of polymer and tend to resist deformation thanks to the strong particle−particle interactions, are no longer effective at large deformations. Therefore, the modulus of the M2 and M5 samples should decrease toward that of *D*, in the limit of extremely large γ_0's. Conversely, the anti-Payne response of A can be interpreted by assuming that its roughly spherical aggregate of particles will be transformed into a more elongated and loosely connected cluster at large deformations. It is quite possible, but we have not tested it, that the modulus of the A sample will also reach a plateau and then drop toward the D value for $\gamma_0 \gg 0.8$.

Figure 7 illustrates what happens when we gradually switch off the particle−particle interactions—not by varying the degree of filler dispersion, but by making the filler and polymer more compatible through changes in the interatomic potentials (cases I, II, and III in Table 1). Again, we observe that there is no significant strain dependence for $\gamma_0 \leq 0.2$. Apart from this common feature, the systems with moderately dispersed (M5) and fully aggregated (A) morphologies seem to behave differently. When we take system M5 and reduce the particle−particle interactions (from case I to case III potentials), we observe a certain drop in small-strain modulus, which becomes similar to that of the systems with either dispersed or fully aggregated particles (D and A, see above). The modulus decreases further at higher strains (Payne-like behavior), so that the M5−III curve is almost a downward-shifted version of M5−I. Instead, a gradual reduction in the particle−particle interactions in the fully aggregated system (curves A−I, A−II, and A−III) does not change significantly the small-strain modulus, which is already rather low. On the other hand, the strain dependence switches from anti-Payne to Payne-like. Thus, the difference between the A−I and A−III moduli at 80% strain is comparable to the difference between the M5−I and M5−III moduli at 10−20% strain. The A−II system, in which only half of the filler atoms are polymer-like, falls nicely between A−I and A−III. This indicates that chemical heterogeneity of the filler surface does not have a specific effect but seems to be averaged out, at least in this case.

Finally, we present a few tests which validate our choices for the DPD thermostat and integration time step. We have conducted nonequilibrium simulations on the unfilled network as well as the D−I and A−I composites, at high frequency and medium strain amplitude ($\nu = 10^{-3}$, $\gamma_0 = 0.1$). Figure 8 presents our results on the average kinetic temperature and the elastic moduli of these systems. A 10-fold decrease of the time step—from $\Delta t = 0.05$ to 0.005—allows an almost perfect temperature control, independently of the value of thermostat parameter γ. When we use $\Delta t = 0.05$, we have a +2% deviation from the programmed temperature when $\gamma = 0.5$ and a −2% deviation when $\gamma = 4.5$. Turning to the elastic muduli, the choice of γ and Δt does not seem to produce significant and systematic effects. There are some small variations in G', but they roughly fall within the estimated error bars. Thus, the main conclusions of the present paper, which is mainly concerned with the strain dependence of the elastic moduli, should be unaffected by these parameters. On the other hand, as recently pointed out by other authors,[39] it is quite possible that the use of a long time step may produce artifacts in some more "fine-grained" quantities

(density profiles and stress at the rubber−filler interface, for example). We plan to address these points in our future work.

4. Conclusions: What Is the Role of Particle−Particle Interactions?

We are now in a position to attempt a summary of our "computer experiments" on the nonlinear viscoelasticity of filled rubbers. Unlike other recent attempts,[26−33] our simulations include some important features of real experimental systems and directly probe the viscoelastic response as a function of shear amplitude and frequency. We believe that the DPD model captures the right degree of coarse-graining for the problem at hand. Also, an important advantage of simulation over experiment is that it allows an independent control over the microscale polymer−filler interactions and the mesoscale morphology of the samples. These aspects are almost always entangled with each other in experimental studies (see however ref 20 for an attempt to resolve them).

What have we learned about the role of particle−particle interactions? The first lesson is that particle−particle interactions have a clearly detectable effect on the modulus (actually, the in-phase component of the dynamics shear modulus), which may be both direct and indirect. The direct effect depends on the observation that, for a given morphology, increasing them always produces a certain increase of the modulus. The indirect effect is due to the fact that different particle−particle interactions, together with other factors such as sample preparation methods, tend to produce morphologies with different degrees of aggregation. In turn, we have observed that this variable has a nonmonotonic effect. Taking the perfectly dispersed sample as reference, the modulus increases up to a certain degree of aggregation (loosely connected network of fillers) but then decreases when this proceeds beyond a certain point, when very large and compact aggregates start to appear. A certain dependence of the small-strain elastic modulus of polymer−filler composites was also seen in FEM simulations by Gusev et al.,[35] where however it was observed to be much stronger for fiber-reinforced than for particle-reinforced composites.

The second lesson from our simulations is that particle−particle interactions may also be responsible for some strain dependence of the modulus. Thus, we find no strain dependence when the particles are perfectly dispersed and some nonlinearity when they are aggregated. However, some characteristics of this behavior seem to be different from those observed experimentally (Payne effect). In some cases we actually observe a strain stiffening of the material (anti-Payne behavior), and even when there is strain softening, this is relatively small in magnitude and tends to occur at rather large deformations ($\gamma_0 \geq 0.2$, as opposed to $\gamma_0 \leq 0.05$ in experimental systems). Therefore, it seems that particle−particle interactions alone cannot explain the Payne effect.

For the future, we plan to extend our simulations by considering systems with higher volume fractions of filler and improve our statistics at small strains through larger samples and longer simulation times. Also, the basic physics of our model will probably need to complicated slightly before our simulations can reproduce the most important features of the behavior of filled rubbers. One possibility is the introduction of a more complicated model for the polymer−filler interface, accounting for debonding or glassy dynamics of the interfacial rubber layer.

Acknowledgment. We thank Giuseppe Allegra for his kind encouragement. This research was financially supported by MIUR-PRIN2005 and by the Fondazione Cariplo. Part of the computer time was made available by Cilea (Milano).

Supporting Information Available: Plots of the out-of-phase component of the complex shear modulus. This material is available free of charge via the Internet at http://pubs.acs.org.

References and Notes

(1) Kraus, G., Ed. *Reinforcement of Elastomers*; Wiley: New York, 1965.
(2) Payne, A. R.; Whittaker, R. E. *Rubber Chem. Technol.* **1971**, *44*, 440−476.
(3) Medalia, A. I. *Rubber Chem. Technol.* **1978**, *51*, 437−523.
(4) Wang, M.-J. *Rubber Chem. Technol.* **1998**, *71*, 520−589.
(5) Smallwood, H. M. *J. Appl. Phys.* **1944**, *15*, 758. Guth, E. *J. Appl. Phys.* **1945**, *16*, 20.
(6) Christensen, R. M. *Mechanics of Composite Materials*; Krieger: Malbar, India, 1991.
(7) Torquato, S. *Random Heterogeneous Materials: Microstructure and Macroscopic Properties*; Springer-Verlag: New York, 2002.
(8) Mondescu, R. P.; Muthukumar, M. *J. Chem. Phys.* **1999**, *110*, 1123−1137.
(9) Huber, G.; Vilgis, T. A. *Macromolecules* **2002**, *35*, 9204−9210.
(10) Muthukumar, M. *J. Chem. Phys.* **1985**, *83*, 3161−3168.
(11) Witten, T. A.; Rubinstein, M.; Colby, R. H. *J. Phys. II* **1993**, *3*, 367−383.
(12) Raos, G. *Macromol. Theory Simul.* **2003**, *12*, 17−23.
(13) Israelachvili, J. N. *Intermolecular and Surface Forces*, 2nd ed.; Academic Press: New York, 1991.
(14) Rong, W. Z.; Pelling, A. E.; Ryan, A.; Gimzewski, J. K.; Friedlander, S. K. *Nano Lett.* **2004**, *4*, 2287−2292. Suh, Y. J.; Friedlander, S. K. *J. Appl. Phys.* **2003**, *93*, 3515−3523. Suh, Y. J.; Ullman, M.; Friedlander, S. K.; Park, K. Y. *J. Phys. Chem. B* **2001**, *105*, 11796−11799.
(15) Kraus, G. J. *Appl. Polym. Sci., Appl. Polym. Symp.* **1984**, *39*, 75.
(16) Huber, G.; Vilgis, T. A.; Heinrich, G. *J. Phys.: Condens. Matter* **1996**, *8*, L409−L412.
(17) Heinrich, G.; Klüppel, M. *Adv. Polym. Sci.* **2002**, *160*, 1−44.
(18) Wolff, S. *Rubber Chem. Technol.* **1996**, *69*, 325−346.
(19) Tsagaropoulos, G.; Eisenberg, A. *Macromolecules* **1995**, *28*, 6067−6077.
(20) Berriot, J.; Montes, H.; Lequeux, F.; Long, D.; Sotta, P. *Macromolecules* **2002**, *35*, 9756−9762. Montes, H.; Lequeux, F.; Berriot, J. *Macromolecules* **2003**, *36*, 8107−8118.
(21) Vilgis, T. A. *Polymer* **2005**, *46*, 4223−4229.
(22) Yurekli, K.; Krishnamoorti, R.; Tse, M. F.; McElrath, K. O.; Tsou, A. H.; Wang, H.-C. *J. Polym. Sci., Part B: Polym. Phys.* **2001**, *39*, 256−275.
(23) Zhang, Q.; Archer, L. A. *Langmuir* **2002**, *18*, 10435−10442.
(24) Maier, P. G.; Göritz, D. *Kautsch. Gummi Kunst.* **1996**, *49*, 18−21.
(25) Sternstein, S. S.; Zhu, A.-J. *Macromolecules* **2002**, *35*, 7262−7273.
(26) Raos, G.; Allegra, G. *J. Chem. Phys.* **2000**, *113*, 7554−7563.
(27) Vacatello, M. *Macromolecules* **2001**, *34*, 1946−1952. Vacatello, M. *Macromol. Theory Simul.* **2003**, *12*, 86−91.
(28) Starr, F. W.; Schrøder, T. B.; Glotzer, S. C. *Macromolecules* **2002**, *35*, 4481−4492.
(29) Smith, G. D.; Bedrov, D.; Li, L.; Byutner, O. *J. Chem. Phys.* **2002**, *117*, 9478−9489. Borodin, O.; Bedrov, D.; Smith, G. D.; Nairn, J.; Bardenhagen, S. *J. Polym. Sci., Part B: Polym. Phys.* **2005**, *43*, 1005−1013.
(30) Brown, D.; Mélé, P.; Marceau, S.; Albérola, N. D. *Macromolecules* **2003**, *36*, 1395−1406.
(31) Kairn, T.; Daivis, P. J.; Ivanov, I.; Bhattacharya, S. N. *J. Chem. Phys.* **2005**, *123*, 194905.
(32) Ozmusul, M. S.; Picu, C. R.; Sternstein, S. S.; Kumar, S. K. *Macromolecules* **2005**, *38*, 4495−4500.
(33) Papakonstantopoulos, G. J.; Yoshimoto, K.; Doxastakis, M.; Nealey, P. F.; de Pablo, J. J. *Phys. Rev. E* **2005**, *72*, 031801.
(34) Gusev, A. A. *Macromolecules* **2001**, *34*, 3081−3093. Bauerle, S. A.; Fredrickson, G. H.; Gusev, A. A. *Macromolecules* **2004**, *37*, 5784−5791.
(35) Gusev, A. A.; Rozman, M. G. *Comput. Theor. Polym. Sci.* **1999**, *9*, 335−337. Lusti, H. R.; Karmilov, I. A.; Gusev, A. A. *Soft Mater.* **2003**, *1*, 115−120.
(36) Groot, R. D.; Warren, P. B. *J. Chem. Phys.* **1997**, *107*, 4423−4435.
(37) Groot, R. D. *Lect. Notes Phys.* **2004**, *640*, 5−38.
(38) Aoyagi, T.; Sawa, F.; Shoji, T.; Fukunaga, H.; Takimoto, J.; Doi, M. *Comput. Phys. Commun.* **2002**, *145*, 267−279. See also the web site http://octa.jp.
(39) Jakobsen, A. F.; Mouritsen, O. G.; Besold, G. *J. Chem. Phys.* **2005**, *122*, 204901. Allen, M. P. *J. Phys. Chem. B* **2006**, *110*, 3823−3820.

(40) Erman, B.; Mark, J. E. *Structure and Properties of Rubberlike Networks*; Oxford University Press: New York, 1997.
(41) Groot, R. D.; Rabone, K. L. *Biophys. J.* **2001**, *81*, 725−736.
(42) The filler blocks actually consists of an alternation of F′ and F″ atoms. These chains should be described as $P_{14}(F'F'')_4P_{14}$. However, F′ = F″ in case I.
(43) When we tried mixing directly 170 P_{14} chains and 600 $P_{14}F_8P_{14}$ chains ($\phi = 0.20$), we did not obtain the near-spherical filler particles described above, but a complex morphology with intertwining wormlike micelles.
(44) Pütz, M.; Kremer, K.; Everaers, R. *Phys. Rev. Lett.* **2000**, *84*, 298−301.
(45) Allen, M. P.; Tildesley, D. J. *Computer Simulation of Liquids*; Clarendon Press: Oxford, 1987.
(46) Clark, A. T.; Lal, M.; Ruddock, J. N.; Warren, P. B. *Langmuir* **2002**, *16*, 6342−6350.
(47) Soddemann, T.; Dünweg, B.; Kremer, K. *Phys. Rev. E* **2003**, *68*, 046702.
(48) The batch average of the stress over the interval $[t, t + \Delta t]$ is output by the program at time $t + \Delta t$. This introduces a small artificial delay in the response of the system to the applied deformation. To minimize this artifact, we associate this batch average with the "instant" $t + \Delta t/2$.
(49) The plots of the out-of-phase components are included in the Supporting Information.

MA061008H